Terahertz-Radiation-Enhanced Emission of Fluorescence from Gas Plasma

Jingle Liu and X.-C. Zhang*

Center for Terahertz Research, Rensselaer Polytechnic Institute, Troy, New York 12180, USA

(Received 23 April 2009; published 2 December 2009)

We report the study of femtosecond laser-induced air plasma fluorescence under the illumination of terahertz (THz) pulses. Semiclassical modeling and experimental verification indicate that time-resolved THz radiation-enhanced emission of fluorescence is dominated by the electron kinetics and the electron-impact excitation of gas molecules or ions. We demonstrate that the temporal waveform of the THz field could be retrieved from the transient enhanced fluorescence, making omnidirectional, coherent detection available for THz time-domain spectroscopy.

DOI: 10.1103/PhysRevLett.103.235002 PACS numbers: 52.25.Os, 32.50.+d, 34.50.Gb, 52.50.Sw

The interaction between electromagnetic waves and laser-induced gas plasma has been extensively studied in most of the spectral regions [1–4]. Electric field measurements and plasma dynamics characterization in gas dc and rf discharge were demonstrated by various schemes of laser-induced fluorescence spectroscopy [5–7]. However, the study in the THz region (0.1 to 10 THz) has been a challenge in the past due to the lack of strong, tabletop THz sources. The low energy of the THz photon promises an *in situ*, noninvasive plasma characterization. The large frequency span of THz pulses recently developed encompasses a wide range of plasma densities and allows highly sensitive probing of the photoionized gas [8–11]. Recent major technical advances in developing intensive THz sources [12–15] have provided us with new opportunities for the investigation of plasma inverse-bremsstrahlung heating [16,17] and electron-impact molecular excitation [18,19] by THz waves. Here, using plasma fluorescence emission, we studied the interaction between an ultrashort THz pulse and plasma by measuring radiation-enhanced emission of fluorescence. Semiclassical modeling of electron motion in the presence of the THz field and electron-impact-excitation of gas molecules is used to calculate the time-dependent plasma response to the THz pulse as a function of electron collision relaxation time and electron-ion recombination rate. The enhanced fluorescence is quadratically dependent on the THz field. The experimental information gathered at different gas pressures agrees with the theoretical calculation. We also demonstrated coherent detection of broadband THz waves by measuring THz radiation-enhanced emission of fluorescence (REEF) from air plasma. Unlike other widely used THz detection techniques [20–22], this method has an omnidirectional emission pattern.

Under the influence of the THz radiation, the electron dynamics in laser-induced plasma is determined by the amplitude and phase of the laser pulse and THz pulse, their delay and gas density. The intense illumination of an ultrashort laser pulse releases free electrons from air molecules by the photoionization. After the passage of the laser pulse, the motion of the elections can be described semiclassically in THz field $\vec{E}_{\mathrm{THz}}(t)$ [3,10]

$$\frac{d\vec{\nu}(t)}{dt} + \frac{\vec{\nu}(t)}{\tau} = -\frac{e}{m}\vec{E}_{\mathrm{Loc}}(t) \tag{1}$$

where $\vec{\nu}(t)$ is the electron velocity, τ is the electron collision relaxation time, and m is the electron mass. $\vec{\nu}(t)/\tau$ is the damping term which is accountable for the energy transfer from electrons to molecules or ions via collisions. $\vec{E}_{\mathrm{Loc}}(t)$ is the local electric field acting on the charges. $\vec{E}_{\mathrm{Loc}}(t) = \vec{E}_{\mathrm{THz}}(t) - \vec{P}/(2\varepsilon_0)$ where $\vec{P}$ is the space-charge polarization [10]. Here we limit our discussion to the case with low plasma density ($\sim 10^{15}$ cm^{-3} or lower) so approximation $\vec{E}_{\mathrm{Loc}} \approx \vec{E}_{\mathrm{THz}}$ can be taken.

During the THz cycle, the electron velocity is increased or decreased depending on the transient direction of the THz field and electron velocity. But the average electron kinetic energy is increased because the electron velocity distribution is symmetric along laser polarization after the ionization, i.e., $\rho(\vec{\nu}(0)) = \rho(-\vec{\nu}(0))$. In laser-induced plasma, there are existing trapped states in the high-lying Rydberg states in atoms and molecules [23]. Those trapped states can be easily ''kicked'' into ionic states via the collision with energetic electrons. After free electrons are heated by the THz radiation, electron-impact ionization of these trapped states leads to the increase of the ion population, which results in enhanced fluorescence emission from molecules or ions in ns [24–26]. Therefore, studying the subsequent molecular fluorescence emission provides information of electron temperature and population of excited molecular states in the presence of the THz radiation [27]. The contribution of the THz field tunneling ionization and THz photoionization are not dominant because of the single-cycle nature of the THz pulse and small THz photon energy (4.1 meV at 1 THz) compared to the ionization energy of the high-lying Rydberg states of molecules ($\sim$ a few hundred meV), respectively.

We calculate the total fluorescence emission $FL(t_d) = FL_b + \Delta FL(t_d)$ as a function of the time delay t_d between the THz pulse peak and the laser pulse peak. Here we

define $t_d > 0$ when the THz pulse is ahead of the laser pulse. FL_b, the plasma fluorescence emission without the THz field, is directly from the laser pulse excitation. Enhanced fluorescence $\Delta FL(t_d)$ takes the form

$$\Delta FL \propto n_e(\beta_{\mathrm{ei}}, t_d)\Big(\sum_{i=1}^{\infty}\langle \Delta E_i(\tau, t_d)\rangle|_{\vec{E}_{\mathrm{THz}}} - \sum_{i=1}^{\infty}\langle \Delta E_i(\tau, t_d)\rangle|_{\vec{E}_{\mathrm{THz}}=0}\Big), \quad (2)$$

where β_{ei} is the electron-ion recombination rate and $\langle \Delta E_i(\tau, t_d)\rangle$ is the average energy which one electron transfers to molecules during ith collision at t_i. The mean fractional loss of electron kinetic energy in a classical collision k is $2mM/(m+M)^2$, where m and M are electron and molecule masses. When $m \ll M$, all directions of electron motion after collision are equally probable and energy transfer in each collision is very small, i.e., $k \approx 2m/M \ll 1$ [28]. Considering the scattering angle probability, the energy transfer

$$\langle \Delta E_i(\tau, t_d)\rangle = \int_{-\infty}^{+\infty}(m\vec{v}^2(0)/2 + m\vec{v}\Delta\vec{v}_1)k(1-k)^{i-1} \times \rho(\vec{v}(0))d\vec{v}(0) + km\sum_{j=1}^{i}\Delta\vec{v}_j{}^2(1-k)^{i-j},$$

where $\Delta\vec{v}_i = -\int_{t_i-\tau}^{t_i} e\vec{E}_{\mathrm{THz}}(t)dt/m$. Because of the $\rho(\vec{v}(0)) = \rho(-\vec{v}(0))$ symmetry, 0. Here the first term accounts for the energy transferred from the initial electron velocity while the second term accounts for the energy transferred from the THz field.

Under gas pressure P, the electron collision relaxation time is $\tau(P) = \tau_0 P_0/P$ where τ_0 is the relaxation time at atmosphere pressure P_0 and is a few hundred femtoseconds [29]. At very low pressure, $\tau(P)$ is much longer than THz pulse duration $\tau_{\mathrm{THz}} \sim 1$ ps and ΔFL can be approximated with $\Delta\vec{v}_1 \neq 0$ and $\Delta\vec{v}_{i>1} = 0$

$$\lim_{\tau \gg \tau_{\mathrm{THz}}} \Delta FL \propto n_e(\beta_{\mathrm{ei}}, t_d)\frac{e^2}{2m}\Big(\int_{t_d+t_\varphi}^{\infty}\vec{E}_{\mathrm{THz}}(t)dt\Big)^2 \propto \vec{A}^2(t_d + t_\varphi). \quad (3)$$

Here $\vec{E}_{\mathrm{THz}}(0) = \vec{E}_{\mathrm{peak}}$. t_φ is the phase delay caused by the plasma formation dynamics at the early stage. Therefore, at low pressure the ΔFL is proportional to the square of the vector potential of the THz pulse at $t_d + t_\varphi$. At very high pressure, $\tau(P) \ll \tau_{\mathrm{THz}}$ and $\vec{E}_{\mathrm{THz}}(t)$ is constant between neighboring collisions, ΔFL becomes

$$\lim_{\tau \ll \tau_{\mathrm{THz}}} \Delta FL \propto n_e(\beta_{\mathrm{ei}}, t_d)\frac{e^2\tau}{2m}\int_{t_d+t_\varphi}^{+\infty}\vec{E}_{\mathrm{THz}}{}^2(t)dt. \quad (4)$$

Therefore ΔFL is proportional to the THz pulse energy at high pressure. In the cases of both Eqs. (3) and (4), the ΔFL carries the information of the THz time-domain waveform.

To test the above semiclassical model, we experimentally investigated the influence of the THz pulse on the plasma. The schematic of the experimental setup is shown in Fig. 1(a). A broadband, single cycle of free space THz radiation with linear polarization and a peak field of 100 kV/cm, generated from a lithium niobate prism using the tilted pulse front scheme [14], is focused into a plasma region which is formed by focusing a 100 μJ femtosecond laser pulse with a center wavelength of 800 nm. The laser pulses propagate collinearly with the THz pulses. The plasma fluorescence spectrum is measured by a monochromator and a photo multiplier tube. As a parallel reference for fluorescence measurement, the THz time-domain waveform was measured by electro-optic (EO) sampling [20].

The THz field dependence of the laser-induced plasma emission spectrum is measured in the spectral range of 320 to 400 nm which contains the second positive band system of N_2 ($C^3\Pi_u - B^3\Pi_g$ transitions at 337, 353, 357, 375, and 380 nm) and the first negative band system of N_2^+

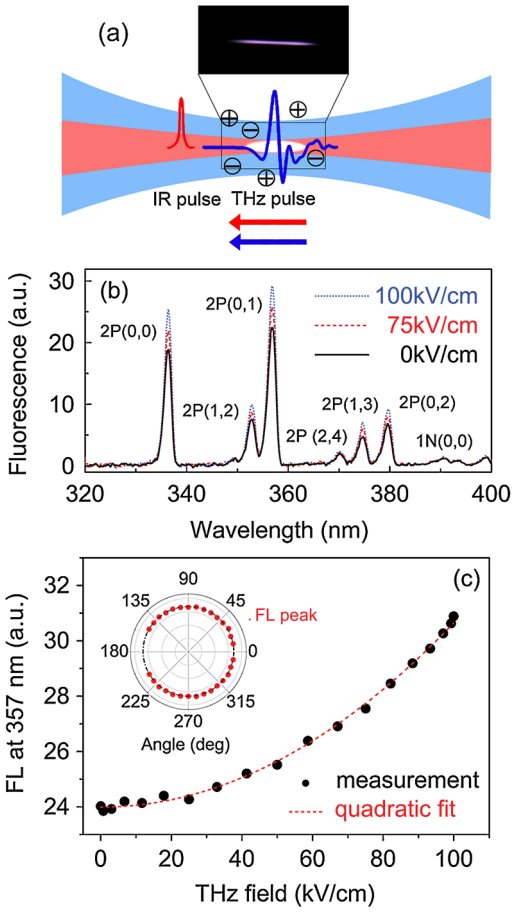

FIG. 1 (color online). (a) Schematics of the interaction between the THz wave and laser-induced plasma. (b) The measured fluorescence spectra versus THz field as $t_d = -1$ ps. Major fluorescence lines are labeled. (c) The measured quadratic THz field dependence of 357 nm fluorescence emission line as $t_d = -1$ ps. Inset: The isotropic emission pattern of THz-REEF.

($B^2\Sigma_u^+ - X^2\Sigma_g^+$ transition at 391 nm) [30]. Figure 1(b) shows that fluorescence emission from both nitrogen molecules and ions is enhanced by the same factor as THz field is increased when $t_d = -1$ ps. In Fig. 1(c), we show that the measured THz field dependence of the total emission FL at the strongest line 357 nm and the quadratical fit when $t_d = -1$ ps. The fact that the ΔFL at all wavelengths is proportional to the THz intensity, agrees with Eq. (4) when high pressure approximation is satisfied at ambient pressure. In the inset of Fig. 1(c), the angular pattern of fluorescence shows an isotropic emission profile. These observations indicate that the THz pulse enhances plasma fluorescence emission through electron heating by the inverse-bremsstrahlung process and subsequent energy transfer to air molecules or ions via inelastic collisions.

Figure 2(a) shows the measured time-resolved $\Delta FL(t_d)$ compared with time-resolved $\vec{E}_{\mathrm{THz}}(t_d)$. When the THz pulse is ahead of the laser pulse in time, $\Delta FL(t_d \gg 1\ \mathrm{ps}) = 0$, which is the same as that without the THz field present. However, the fluorescence shows a rapid increase when two pulses are shifted close enough that the tail of the THz pulse starts to temporally overlap with the laser pulse. At the larger negative delay, the slow decrease of the $\Delta FL(t_d)$ is due to the decrease of electron density by electron-ion recombination. This is confirmed by the agreement with the calculated temporal evolution of electron density $n_e(t) = n_e(0)/(1 + n_e(0)\beta_{\mathrm{ei}}t)$ [31], where the initial electron density $n_e(0) \sim 10^{16}\ \mathrm{cm}^{-3}$ by assuming $\beta_{\mathrm{ei}} = 6.1 \times 10^{-12}\ \mathrm{m}^3/\mathrm{s}$ [32]. This $n_e(0)$ might be overestimated because β_{ei} used here was measured at 29 torr and effective β_{ei} at atmospheric pressure is expected to be higher considering larger population of complex ions and larger three body recombination rate. In a separate experiment, the plasma density was measured to be in range of 10^{14} to $10^{15}\ \mathrm{cm}^{-3}$ by using THz time-domain spectroscopy [10]. The electron densities in a laser filament were measured by several groups [31,33,34].

The width of the rising edge is comparable with the THz pulse duration as shown in the expanded scale in Fig. 2(b). $\Delta FL(t_d)$ peaks when the laser pulse is temporally coincident with the beginning of the THz pulse. The highest enhancement ratio $\Delta FL(t_d)/FL(t_d)$ is observed to reach 80% with a THz peak field of 100 kV/cm. In the bottom curves, the time derivative of the enhanced fluorescence is found to be proportional to the square of the THz field with a constant phase delay $d\Delta FL(t_d)/dt_d \propto \vec{E}_{\mathrm{THz}}{}^2(t_d + t_\varphi)$ which agrees with Eq. (4) for high pressure approximation. The experimental value of t_φ is about 100 fs at laser excitation intensity 10^{13}–$10^{14}\ \mathrm{W/cm}^2$.

To verify the general calculation of ΔFL in Eq. (2), THz-REEF experiments in pure nitrogen gas were carried out at different gas pressures. Figure 3(a) plots $\Delta FL(t_d)$ at different pressures while the laser excitation intensity remains constant. The $\Delta FL(t_d)$, which is proportional to the product of n_e and $m\sum_{i=1}^{\infty}\Delta\vec{\nu}_i{}^2$, reaches a maximum at a

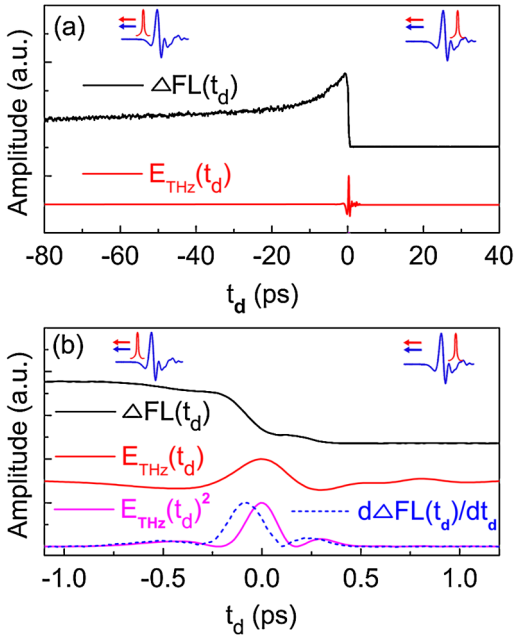

FIG. 2 (color online). (a) The time-resolved THz-REEF $\Delta FL(t_d)$ and THz field $\vec{E}_{\mathrm{THz}}(t_d)$. (b) The time-resolved $\Delta FL(t_d)$, $\vec{E}_{\mathrm{THz}}(t_d)$, $d\Delta FL(t_d)/dt_d$, and $\vec{E}_{\mathrm{THz}}{}^2(t_d)$ on the rising edge in the expanded scale of (a). All curves are normalized and offset for clarity.

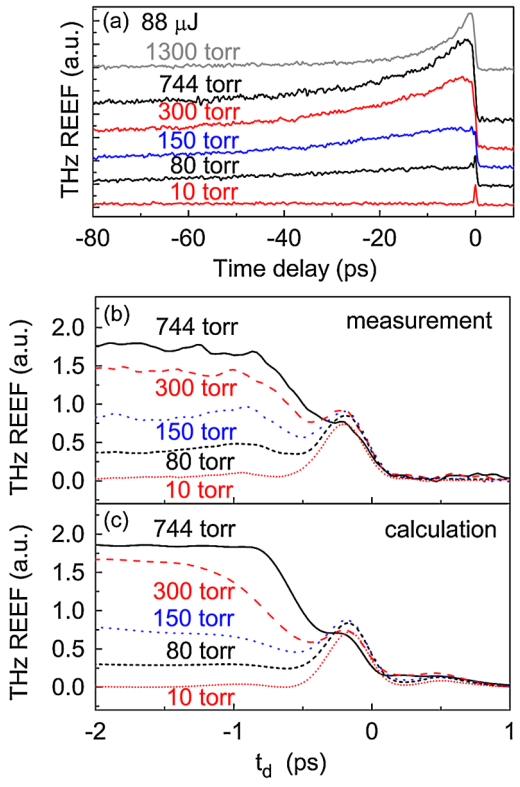

FIG. 3 (color online). The THz pulse enhanced fluorescence in nitrogen at a pressure range of 1300 to 10 torr. (a) Measured time-resolved $\Delta FL(t_d)$ (offset for clarity). (b) Expanded scale of the measured time-resolved $\Delta FL(t_d)$ on the rising edge. (c) Calculated time-resolved $\Delta FL(t_d)$ on the rising edge.

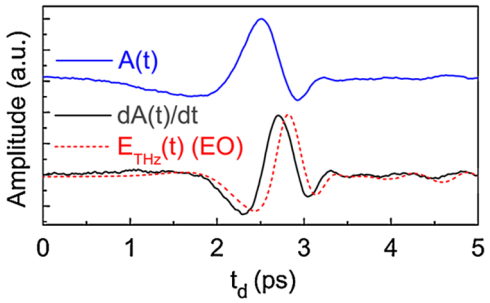

FIG. 4 (color online). Vector potential $\vec{A}(t_d)$ of THz pulse measured by THz REEF and the $d\vec{A}(t_d)/dt_d$ compared with the THz waveform measured by EO detection.

few hundred torr as n_e monotonically increases with the pressure and $m\sum_{i=1}^{\infty}\Delta\vec{v}_i^{\,2}$ depends on pressure in a more complicated way. On the slowly falling edge, the decrease of ΔFL with more negative t_d shows significant pressure dependence. This is attributed to the electron density dependence of the electron-ion recombination process [31]. Figures 3(b) and 3(c) show the measured $\Delta FL(t_d)$ and the calculated $\Delta FL(t_d)$ from Eq. (2) on the rising edge in the expanded scale, respectively. τ_0 is estimated to be 350 fs. In the calculation at each pressure, $\Delta FL(t_d)$ is normalized according to the experimental results. The agreement found in Figs. 3(b) and 3(c) further supports the proposed mechanism.

We also demonstrated the capability of the THz spectroscopy using REEF. The linear dependence of ΔFL on $\vec{E}_{\mathrm{THz}}{}^2$ at ambient pressure in Eq. (4), provides a method for incoherent THz detection with temporal resolution determined by the ionizing pulse envelope. The coherent detection using REEF is also applicable if an external 20 kV/cm bias parallel with $E_{\mathrm{THz}}(t)$ is applied on the plasma as a local oscillator E_{LO}. The resulting ΔFL is

$$\Delta FL \propto \tau \int_{t_d+t_\varphi}^{+\infty} 2\vec{E}_{\mathrm{LO}}\vec{E}_{\mathrm{THz}}(t)dt \propto \vec{E}_{\mathrm{LO}}\vec{A}(t_d + t_\varphi). \quad (5)$$

In this manner, the THz waveform can be retrieved from the derivative of $\vec{A}(t_d)$, with a phase delay t_φ. Figure 4 shows measured $\vec{A}(t_d)$ and good agreement between the THz waveform calculated from $d\vec{A}(t_d)/dt_d$ and that measured by EO sampling.

In conclusion, we studied the interaction between a THz pulse and plasma by investigating THz radiation-enhanced emission of fluorescence from laser-induced plasma in gas. Both theoretical and experimental studies show that the free-electron dynamics under the influence of the THz field can be described by electron heating and electron-impact-excitation of gas molecules or ions. The THz-enhanced-fluorescence intensity carries THz waveform information. The demonstrated omnidirectional broadband coherent THz wave detection could be potentially extended to other spectral regions and is ideal for standoff detection.

The authors thank Nicholas Karpowicz, Etienne Gagnon, and Jianming Dai for the technical assistance and scientific discussions and acknowledge support from the Department of Homeland Security through the DHS-ALERT Center under Grant No. 2008-ST-061-ED0001.

*zhangxc@rpi.edu

[1] W. Woo and J. S. DeGroot, Phys. Fluids **27**, 475 (1984).
[2] P. Gibbon and E. Forster, Plasma Phys. Controlled Fusion **38**, 769 (1996).
[3] W. L. Kruer, *The Physics of Laser Plasma Interactions* (Westview Press, CO, 2003).
[4] J. Filevich *et al.*, Appl. Opt. **43**, 3938 (2004).
[5] C. A. Moore, G. P. Davis, and R. A. Gottscho, Phys. Rev. Lett. **52**, 538 (1984).
[6] E. Wagenaars, M. D. Bowden, and G. M. W. Kroesen, Phys. Rev. Lett. **98**, 075002 (2007).
[7] U. Czarnetzki, D. Luggenhölscher, and H. F. Döbele, Phys. Rev. Lett. **81**, 4592 (1998).
[8] B. H. Kolner *et al.*, IEEE J. Sel. Top. Quantum Electron. **14**, 505 (2008).
[9] S. P. Jamison *et al.*, J. Appl. Phys. **93**, 4334 (2003).
[10] Z. Mics *et al.*, J. Chem. Phys. **123**, 104310 (2005).
[11] T. Kampfrath *et al.*, Chem. Phys. Lett. **429**, 350 (2006).
[12] R. Kohler *et al.*, Nature (London) **417**, 156 (2002).
[13] D. J. Cook and R. M. Hochstrasser, Opt. Lett. **25**, 1210 (2000).
[14] K. L. Yeh *et al.*, Appl. Phys. Lett. **90**, 171121 (2007).
[15] T. Bartel *et al.*, Opt. Lett. **30**, 2805 (2005).
[16] J. F. Seely and E. G. Harris, Phys. Rev. A **7**, 1064 (1973).
[17] L. Schlessinger and J. Wright, Phys. Rev. A **20**, 1934 (1979).
[18] A. V. Phelps, Rev. Mod. Phys. **40**, 399 (1968).
[19] V. A. Shakhatov and Yu. A. Lebedev, High Energy Chem. **42**, 170 (2008).
[20] Q. Wu, M. Litz, and X.-C. Zhang, Appl. Phys. Lett. **68**, 2924 (1996).
[21] D. Grischkowsky *et al.*, J. Opt. Soc. Am. B **7**, 2006 (1990).
[22] J. Dai, X. Xie, and X.-C. Zhang, Phys. Rev. Lett. **97**, 103903 (2006).
[23] A. Talebpour, Y. Liang, and S. L. Chin, J. Phys. B **29**, 3435 (1996).
[24] A. Iwasaki *et al.*, Appl. Phys. B **76**, 231 (2003).
[25] H. L. Xu *et al.*, Chem. Phys. **360** 171 (2009).
[26] A. E. Martirosyan *et al.*, J. Appl. Phys. **96**, 5450 (2004).
[27] T. Fukuchi, R. F. Wuerker, and A. Y. Wong, J. Appl. Phys. **75**, 7237 (1994).
[28] E. W. McDaniel, *Collision Phenomena in Ionized Gases* (John Wiley & Sons, Inc., New York, 1964).
[29] M. Mlejnek, E. M. Wright, and J. V. Moloney, Phys. Rev. E **58**, 4903 (1998).
[30] A. Talebpour, S. Petit, and S. L. Chin, Opt. Commun. **171**, 285 (1999).
[31] S. Tzortzakis *et al.*, Opt. Commun. **181**, 123 (2000).
[32] B. B. Bryan, R. B. Holt, and O. Oldenberg, Phys. Rev. **106**, 83 (1957).
[33] H. Schillinger and R. Sauerbrey, Appl. Phys. B **68**, 753 (1999).
[34] J. Kasparian, R. Sauerbrey, and S. L. Chin, Appl. Phys. B **71**, 877 (2000).